Dissecting TGF-β-induced glioblastoma invasion with engineered hyaluronic acid hydrogels Ⓕ

View Online   Export Citation   CrossMark

Kwasi Yeboa Amofa,[1,2,3] Ⓘ Katherine Michelle Patterson,[2] Ⓘ Jessica Ortiz,[1,2,3] Ⓘ and Sanjay Kumar[1,2,3,4,a)] Ⓘ

AFFILIATIONS

[1]University of California, Berkeley–University of California, San Francisco Graduate Program in Bioengineering, Berkeley, California 94720, USA
[2]Department of Bioengineering, University of California, Berkeley, California 94720, USA
[3]Department of Bioengineering and Therapeutic Sciences University of California San Francisco, California 94158, USA
[4]Department of Chemical and Biomolecular Engineering, University of California, Berkeley, California, 94720, USA

Note: This paper is part of the special issue on Physical Sciences Approaches to Cancer Research.
[a)]Author to whom correspondence should be addressed: skumar@berkeley.edu

ABSTRACT

Glioma stem cells (GSCs) contribute to rapid cellular invasion in glioblastoma (GBM). Transforming growth factor-β (TGF-β) has been strongly implicated in supporting key GSC functions, including stemness, immunosuppression, and resistance. Although TGF-β is well-known as a driver of cancer invasion, how TGF-β supports the invasion of GSCs is not well understood. Progress in understanding mechanisms of TGF-β-driven invasion in GSC-derived tumors has been limited by an absence of three-dimensional (3D) culture systems that support TGF-β-stimulated invasion. Here, we show that 3D hyaluronic acid (HA) matrices can address this need. We perform bioinformatic analysis of human glioma datasets, which reveals progressive enrichment of TGF-β-related gene expression with increasingly aggressive glioma grade and GBM subtype. We then experimentally screen the invasion of a panel of human GSC spheroids through a set of 3D matrix systems, including collagen I, Matrigel, and HA, and find that only HA recapitulates TGF-β-induced invasion. We then show that GSCs differ in their ability to invade HA in a way that can be predicted from TGF-β receptor 2 expression and SMAD2 phosphorylation. GSC spheroid invasion depends strongly on the presence of RGD peptides on the HA backbone but is surprisingly independent of matrix metalloprotease degradability. Finally, we demonstrate that TGF-β stimulates invasion through SMAD-dependent signaling, consistent with recent observations that TGF-β/SMAD signals drive tumor microtube formation and invasion. Our work supports further development of HA as a matrix platform for dissecting contributions of TGF-β and other cytokines to GBM invasion and screening of cytokine-dependent invasion in human tumors.

INTRODUCTION

Glioblastoma (GBM) is an incurable primary brain tumor marked by rapid cellular invasion into the surrounding brain tissue, which is in turn promoted by a combination of biochemical and biophysical factors within the tumor microenvironment (TME).[1,2] Biochemical factors found in the TME include secretory cytokines, such as transforming growth factor-β (TGF-β), tumor necrosis factor-α (TNF-α), and interleukins, many of which can prime tumor cells for invasion through receptor-mediated signaling.[3–5] Successful invasion also typically involves engagement with the extracellular matrix (ECM) through integrins, CD44, and other adhesion receptors, as well as remodeling of the ECM through protease degradation and nascent ECM deposition.[6–9]

Over the past two decades, glioma stem cells (GSCs) have been increasingly implicated in driving GBM initiation, growth, recurrence, and resistance.[10,11] Although the importance of GSCs in invasion is less well appreciated, GSCs are found at the invasive peritumoral region of GBMs and can directly contribute to the evasion of therapeutic agents and seeding of secondary tumors.[12] The cytokine TGF-β appears to play a particularly potent role in the maintenance of GSC stem-like characteristics and tumor-initiating capacity, with TGF-β-dependent signaling contributing to local immunosuppression and resistance to ionizing radiation and chemotherapies.[13–17] While TGF-β signaling regulates GSC properties, how TGF-β stimulates GSC invasion specifically has been minimally explored,[18–20] which is in part due to a lack of in vitro culture platforms that can enable systematic

dissection of intracellular and extracellular regulators of TGF-β-mediated invasion. The development and application of such platforms could offer new mechanistic insight into how TGF-β (and, by extension, other cytokines) drives GBM pathology, uncover new prognostic markers and therapeutic targets, and establish a foundation for personalized screening.

Traditional *in vitro* culture platforms to study invasion include two-dimensional (2D) tissue culture dishes and Boyden chamber assays. While these simplified paradigms have enabled novel insight into GBM pathology, they lack the full three-dimensional (3D) ECM microenvironment characteristic of tissue. To address this limitation, there has been a growing effort to model invasion using 3D *in vitro* culture models, including embedding tumor spheroids within 3D hydrogels, which are typically composed of tissue ECM preparations or purified ECM proteins such as collagen I.[21,22] While native ECM-based hydrogels incorporate important structural and bioactive features of tissue ECMs, they are often heterogeneous, incompletely defined, and not amenable to precise modulation of biophysical properties. These needs have paved the way for engineered ECMs that enable tight control of viscoelastic properties and presentation of bioactive peptides for adhesion, capture of growth factors, and protease digestion. 3D invasion platforms may be built from ECM-derived biopolymers, such as alginate or hyaluronic acid (HA), or fully synthetic polymers, such as polyethylene glycol (PEG).[23–25]

HA is an especially attractive platform for modeling GBM invasion. HA is the most abundant matrix component in normal brain and plays a critical role in defining brain structure and mechanics. Moreover, HA is highly enriched in GBM relative to healthy brain tissue, with the most aggressive forms of gliomas exhibiting greater levels of HA and altered HA molecular weight.[2,26] HA-based adhesive signaling through CD44 and other receptors can drive GBM progression and infiltration into brain tissue.[2,8,27] HA also retains the chemical versatility of synthetic polymers as it contains multiple orthogonal functional groups (e.g., hydroxyl, carboxyl) that can be exploited for conjugation of cross-linking agents and bioactive peptides.[27] To this end, we and others have productively used HA-based scaffolds to model, deconstruct, and conduct molecular screens in GBM.[28–33] Additionally, HA-CD44 signaling can also directly and indirectly modulate TGF-β signaling. For example, CD44 has been shown to directly bind and stimulate signaling through TGF-β receptor I, with TGF-β receptor I reciprocally phosphorylating and activating CD44 to promote HA-based adhesion and migration.[34–37] Thus, HA is not only an ideal material for modeling GBM invasion, but is particularly suitable for investigating contributions of TGF-β to the process.

Here, we combine engineered HA hydrogels, bioinformatic analysis, GSC culture, and mechanistic perturbations to investigate the interplay between TGF-β signaling and HA scaffold properties in driving invasion. We classify GSCs according to their ability to invade HA in spheroid culture and correlate that invasive potential to the expression of elements within the TGF-β signaling pathway. We also identify matrix conditions necessary for invasion, with invasion being strongly reliant on the presence of integrin-ligating peptides but surprisingly independent of proteolytic degradability. Finally, we show that TGF-β-induced GSC invasion in HA is mediated by SMAD2 phosphorylation, which is amplified when RGD peptides are conjugated to the HA backbone.

RESULTS

Expression of TGF-β-related transcripts correlates with disease aggression in human gliomas

Although much direct and indirect evidence supports a role for TGF-β in GBM invasion, many of these studies are preclinical in nature. Thus, we began by querying The Cancer Genome Atlas (TCGA) and the Repository for Molecular Brain Neoplasia Data (Rembrandt) to confirm if tumor aggressiveness is correlated with enhanced expression of TGF-β-associated transcripts in a broad cohort of human GBMs. Using the GlioVis (http://gliovis.bioinfo.cnio.es/) to access the Rembrandt patient dataset, we first assessed the relative expression of TGF-β ligands (TGFB1, TGFB2) and associated receptors (TGFBR1, TGFBR2) in different glioma grades (oligodendroglioma, astrocytoma, and GBM) relative to normal brain. The highest grade glioma, GBM, exhibited the highest expression of both TGF-β ligands and receptors [Fig. 1(a)].

We then focused our analysis on GBM. GBM tumors have been transcriptionally classified into subtypes (proneural, classical, and mesenchymal), with mesenchymal-subtype tumors typically associated with more aggressive phenotypes and poorer patient survival time.[38] We first compared the expression of TGF-β ligands (TGFB1 and TGFB2) and associated receptors (TGFBR1 and TGFBR2) in mesenchymal-subtype tumors to the proneural subtype, which is associated with a more favorable patient survival time but often recurs as the mesenchymal subtype.[38] Mesenchymal tumors expressed higher levels of both TGF-β ligands and receptors relative to proneural tumors [Fig. 1(b)]. Next, we assembled a panel of TGF-β-responsive genes in glioma tissue from the literature and compared the expression of these genes in mesenchymal and proneural GBMs.[20,39] Mesenchymal GBMs expressed most of these TGF-β targets at higher levels than proneural GBMs [Fig. 1(c)]. We also broadened our search to TGF-β-related genes reported in the KEGG Pathway Database and Molecular Signatures Database (MSigDB) and found a few genes upregulated in the mesenchymal GBM tissue compared to the proneural GBM tissue (Fig. S6). Thus, the expression of TGF-β pathway components and transcriptional targets correlates with increasing glioma grade and is further enhanced in GBM subtypes considered most aggressive.

HA matrix supports TGF-β-responsive invasion in a GSC subtype-specific fashion

Given that HA is highly abundant in glioma tissue and can influence TGF-β signaling, we next investigated the use of HA as a platform for studying TGF-β-induced GSC invasion. We first selected an HA hydrogel in which RGD-based peptides were conjugated to the HA backbone and where hydrogel assembly was mediated by a protease-degradable crosslinker to achieve a stiffness of ∼450 Pa. Our parameter selections were guided by our past HA formulations for studying GBM invasion.[8,29,32] We then selected a panel of patient GSCs derived from mesenchymal (GSC20 and GSC28) and proneural (GSC262 and GSC295) tumors and subjected spheroids of each GSC type to 3D invasion assays in engineered HA matrices. In the absence of TGF-β stimulation, all GSC spheroids remained circumscribed and did not invade, as qualitatively defined by the absence of protrusions, multicellular fingers, or escaped cells from the spheroid [Figs. 2(b) and 2(c)]. This noninvasive phenotype persisted over 14 days of culture in HA
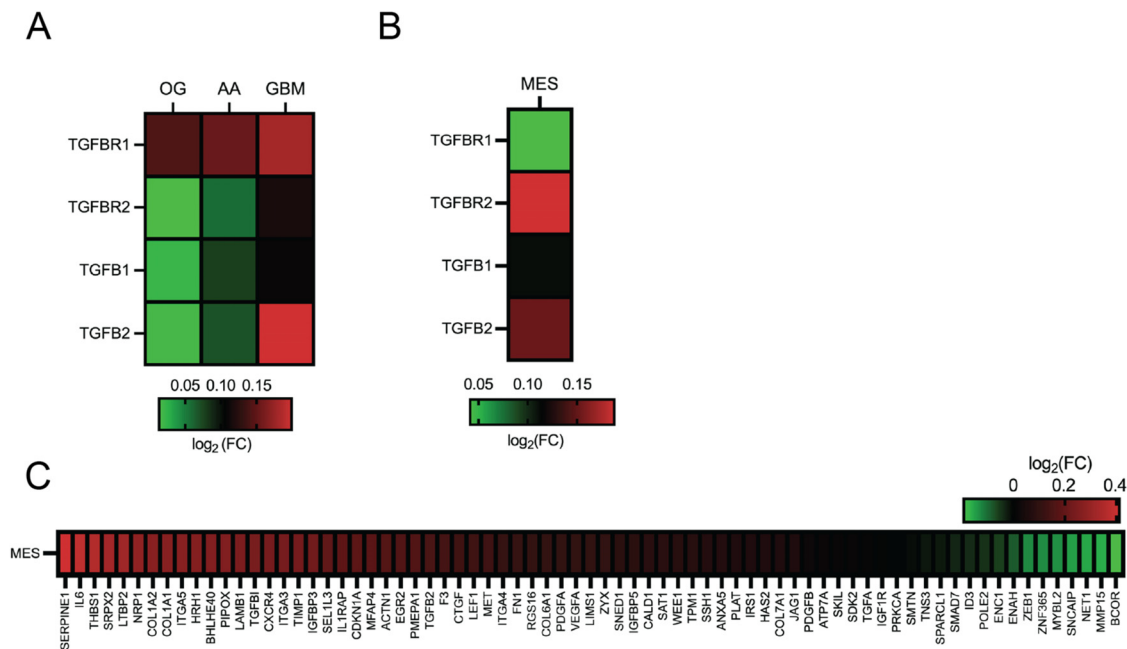
FIG. 1. Expression of TGF-β-related transcripts correlates with disease aggression in human gliomas. (a) Correlation of TGF-β receptors and ligand expression with glioma grade. Oligodendroglioma (OG), astrocytoma (AA), and glioblastoma (GBM) expression of TGF-β ligands and receptors normalized to non-tumor tissue. (b) Expression of TGF-β ligands and receptors in GBM mesenchymal tumors (Mes). (c) Expression of TGF-β target genes (curated from literature) in mesenchymal GBM tumors. In (b) and (c), the expression of each gene was normalized to values for proneural tumors. In (a)–(c), expression data were acquired from TCGA using Gliovis.

(Fig. S1). Despite the absence of invasion, the spheroids continued to grow in volume indicating ongoing proliferation (Fig. S1). Interestingly, we observed that the noninvasive phenotype of the GSC20 and GSC28 in HA was independent of stiffness over a range of 100 Pa–1.2 kPa, which nominally brackets the stiffness range of brain and glioma tissue (Fig. S8).[40–42] The addition of the TGF-β1 ligand stimulated GSC invasion through extended and branched protrusion into the matrix [Fig. 2(b)], although only for a subset of GSCs tested. Notably, the responsive GSCs (GSC20 and GSC28) were both derived from mesenchymal tumors [Fig. 2(b)], while the non-responsive GSCs (GSC295 and GSC262) were both derived from proneural tumors [Fig. 2(c)]. Thus, in this limited subset of GSCs, HA recapitulates the expected hierarchy of subtype-specific invasive behaviors.

To determine whether other commonly used 3D ECM platforms can similarly support subtype-specific TGF-β invasion, we repeated GSC spheroid invasion studies in two naturally derived matrices: collagen I and Matrigel. We chose these matrices because of their common use in tumor invasion studies rather than their mimicry of brain tissue; the brain is typically understood to be collagen I-poor relative to other tissues and Matrigel is derived from mouse sarcoma basement membrane.[43,44] In contrast to HA matrix, all the GSCs rapidly invaded collagen I and Matrigel matrices within 24 h of seeding, with or without TGF-β1 stimulation [Figs. 2(e) and 2(f) and 2(h) and 2(i)]. In collagen, GSC migratory protrusions were linear and directional, whereas in Matrigel, protrusions displayed a diversity of invasion morphologies, including directional, branched, and single cell modalities that varied across GSC lines. Again, these morphologies were present with and

without TGF-β1 stimulation. Nonetheless, collagen did preserve some differences across GSC lines previously identified as TGF-β-responsive/non-responsive in HA (GSC20, GSC28), including longer protrusions for these GSCs under TGF-β stimulation, contributing to a modest TGF-β-dependent increase in the spheroid invasion index.

TGF-β-induced invasion of GSCs in HA is mediated by SMAD phosphorylation

To gain additional insight into the mechanistic origins of the differential HA invasion response across GSCs, we measured the expression of the TGF-β receptors TGFBR1 and TGFBR2 with qPCR. The expression of TGFBR2, but not TGFBR1, was higher in responsive GSCs (GSC20 and GSC28) relative to nonresponsive GSCs (GSC295 and GSC262) [Figs. 3(a) and 3(b)]. Interestingly, when assessing the levels of TGFBR1 and TGFBR2 expression in each of the GSC lines, we found that the relative expression of TGFBR2 was two to threefold higher than the expression of TGFBR1 in the responsive GSCs (GSC20 and GSC8). This contrasted with the non-responsive GSCs (GSC295 and GSC262), where TGFBR2 expression was two to nine fold lower than TGFBR1 expression [Fig. 3(c)].

Having correlated TGF-β responsiveness with TGFBR2 expression, we next investigated whether this correlation extended to TGF-β pathway effectors by measuring SMAD2 phosphorylation. Responsive GSCs exhibited SMAD2 phosphorylation [Fig. 3(d)] when treated with the TGF-β1 ligand, whereas the nonresponsive GSCs lacked SMAD2 phosphorylation [Fig. 3(e)]. To test the functional contributions of
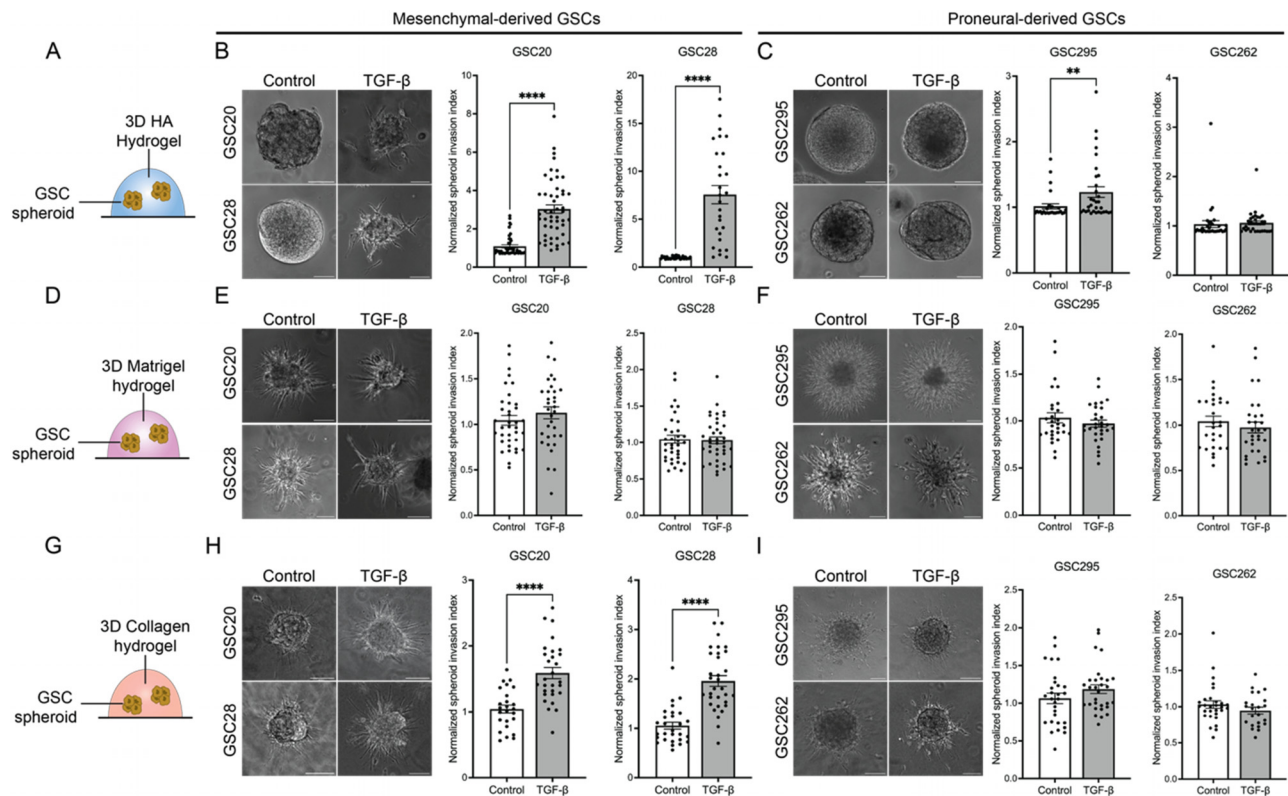
FIG. 2. HA matrix supports TGF-β-responsive invasion in a GSC subtype-specific fashion. (a) Schematic of HA GSC spheroid invasion assay. (b) and (c) GSC spheroid invasion in HA. GSCs were cultured in HA with or without TGF-β stimulation. Data represent n = 44 and 50 spheroids (GSC20), 31 and 28 spheroids (GSC28), 27 and 32 spheroids (GSC295), and 32 and 33 spheroids (GSC262) for control and TGF-β stimulation conditions, respectively. Values display mean ± standard error of the mean (SEM). (d) Schematic of GSC spheroid invasion assay in Matrigel. (e) and (f) GSC spheroid invasion in Matrigel. GSCs were in Matrigel cultured with or without TGF-β stimulation. Data represent n = 37 and 33 spheroids (GSC20), 35 and 39 spheroids (GSC28), 29 and 30 spheroids (GSC295), and 28 and 30 spheroids (GSC262) for control and TGF-β stimulation conditions, respectively. Values display mean ± SEM. (g) Schematic of GSC spheroid invasion assay in collagen. (h) and (i) GSC spheroid invasion in collagen. GSCs were in collagen cultured with or without TGF-β stimulation. Data represent n = 25 and 29 spheroids (GSC20), 28 and 32 spheroids (GSC28), 29 and 30 spheroids (GSC295), 29 and 23 spheroids (GSC262) for control and TGF-β stimulation conditions, respectively. Values display mean ± SEM $^{*}p < 0.033$, $^{**}p < 0.002$, $^{***}p < 0.0002$, and $^{****}p < 0.00001$ (Mann–Whitney test). Scale bar: 100 μm.

SMAD phosphorylation to invasion, we repeated our 3D HA tumor spheroid invasion studies in the presence of a SMAD2 inhibitor (Galunisertib) that has been explored clinically to treat GBM.[45] Galunisertib treatment suppressed TGF-β-stimulated invasion by sixfold for GSC20 and threefold for GSC28, confirming that TGF-β-induced SMAD2 phosphorylation drives invasion [Figs. 3(f) and 3(g)]. This finding corroborates recent evidence pointing to SMAD activation as a mediator of TGF-β-induced formation of tumor microtubes, which support GBM invasion *in vivo*.[20]

TGF-β-induced GSC invasion in HA matrices requires conjugation of RGD peptides

Finally, we sought to deconstruct matrix-based contributions to TGF-β-stimulated 3D cell motility in HA. 3D invasion is supported by a combination of cell-matrix adhesion and ECM remodeling, including matrix digestion. In our engineered HA platform, we have previously established that at least two adhesive systems contribute to adhesion: binding of CD44 to the HA backbone and binding of

integrins to HA-conjugated RGD peptides.[7,8] Additionally, our HA matrix is crosslinked with a peptide crosslinker that may be cleaved by matrix metalloproteinases (MMP) [Fig. 4(a)]. To understand how these three modalities contribute to TGF-β-stimulated invasion, we first measured transcriptional changes of responsive GSCs (GSC20 and GSC28) cultured in our HA platform with and without TGF-β stimulation via qPCR. We selected a set of genes related to ECM adhesion and remodeling including hyaluronidases, HA synthase, MMPs, and integrin subunits expected to be relevant in our HA matrix. We observed an overall increase in expression of all the genes with the highest fold change captured in MMP2 and ITGB3 for both GSC20 and GSC28 cultured in HA under TGF-β stimulation [Figs. S3(c) and S4(c)]. Interestingly, we noticed that genes relating to matrix degradation (MMP2 and HYAL1) were upregulated in both GSCs, while some genes relating to matrix synthesis (HAS2) and adhesion (ITGAV and ITGB1) were only upregulated in GSC28 but not GSC20. CD44 expression was not altered with TGF-β treatment in either cell line [Figs. S3(c) and S4(c)]. We further compared these findings to patient transcriptomic data based on GBM subtype and found an upregulation
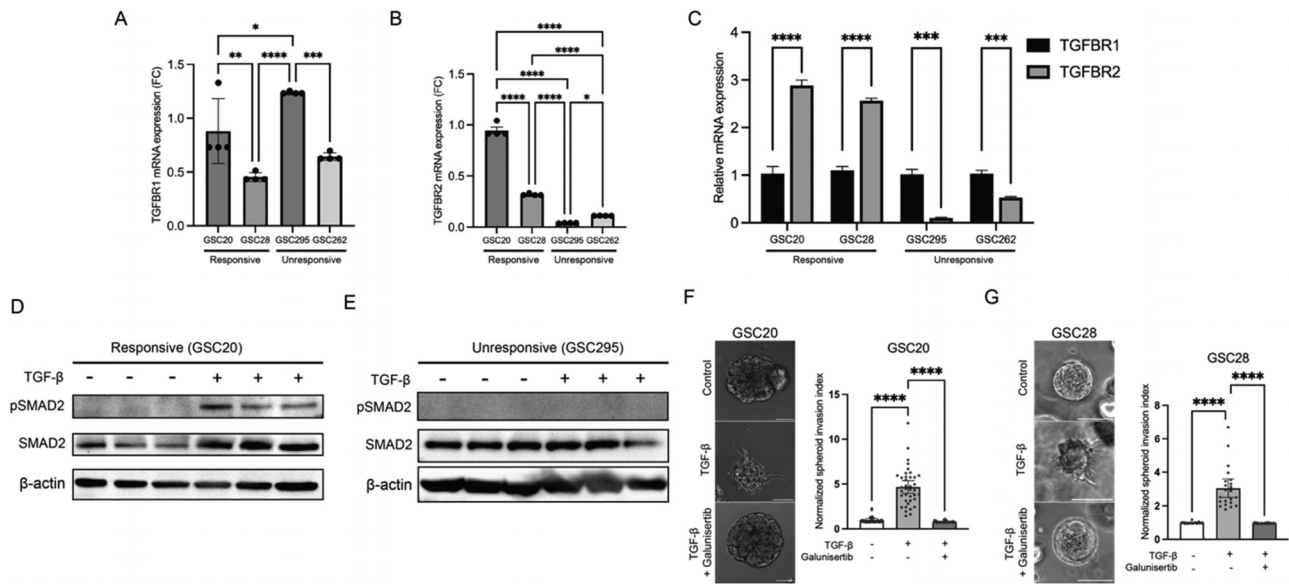
FIG. 3. TGF-β-induced invasion of GSCs in HA is mediated by SMAD phosphorylation. (a) Relative TGFBR1 mRNA expression in GSC20, GSC28, GSC295, and GSC262. Expression from all GSCs was normalized to GSC20. n = 4 biological replicates. (b) Relative TGFBR2 mRNA expression in GSC20, GSC28, GSC295, and GSC262. n = 4 biological replicates. Expression from all GSCs was normalized to GSC20. (c) TGBR2 mRNA expression relative to TGFBR1 expression. The expression of TGFBR1 was used to normalize TGFBR2 expression within each of the GSCs used (GSC20, GSC28, GSC295, and GSC262). n = 4 biological replicates. (d) and (e) Comparison of SMAD2 activity from GSCs with and without TGF-β treatment. Western blot probing pSMAD, SMAD2, and β-actin expression in representative TGF-β-responsive (d) and non-responsive (e) GSCs. Western blots are representative example from n = 3 biological replicates for both responsive and non-responsive GSCs. (f) and (g) SMAD2 inhibition of TGF-β stimulated invasion. Spheroid invasion of GSC20(F) andGSC28 (g) in HA under TGF-β stimulation, with or without SMAD2 inhibitor (galunisertib). Data represent n = 28 (control), 38 (TGF-β), and 34 (TGF-β + galunisertib) spheroids for GSC20 and 24 (control), 22 (TGF-β), and 27 (TGF-β + galunisertib) spheroids for GSC28. *p < 0.033, **p < 0.002, ***p < 0.0002, and ****p < 0.000 01 by (a) and (b) one way ANOVA with Tukey multiple comparison test; (c) Unpaired t-test; and (e) Kruskal–Wallis test with Dunn's multiple comparison test. Values display mean ± SEM. Scale bar: 100 μm.

of these genes in mesenchymal tumors compared to proneural tumors (Fig. S7). Only HYAL1 was upregulated in proneural tumors (Fig. S7). Furthermore, we selected another gene set that is commonly reported to be associated with the GBM mesenchymal signature, is targetable by TGF-β, and includes multiple regulators of ECM remodeling.[46–51] We found that all genes in this set were upregulated in both GSCs when

treated with TGF-β in HA, except for CHI3L (YLK-40), which exhibited reduced expression in GSC20 [Fig. S3(a) and S4(a)].

Next, we subjected GSC20 and GSC28 to HA tumor spheroid invasion assays in which we either included or excluded RGD peptides from the HA backbone and used either protease-degradable or non-degradable peptide crosslinkers. When MMP degradability was
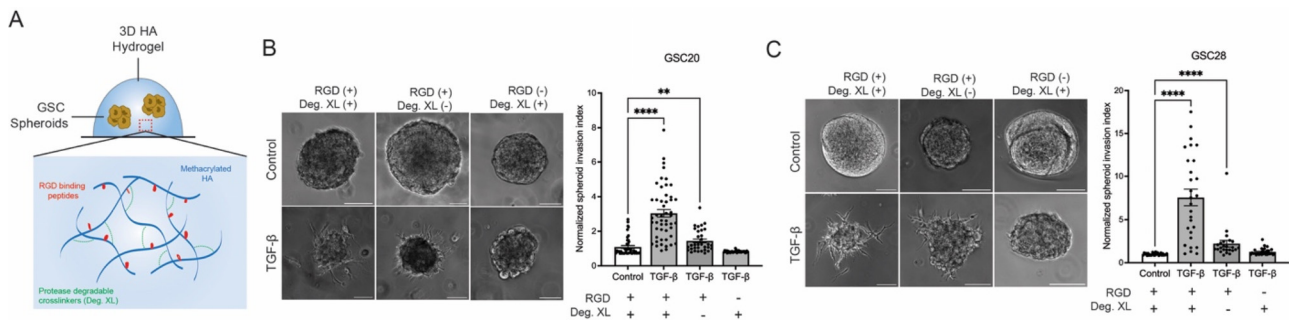

FIG. 4. TGF-β-induced GSC invasion in HA matrices requires conjugation of RGD peptides. (a) Schematic of engineered HA matrix showing RGD peptides and protease-degradable crosslinkers. (b) and (c) TGF-β-stimulated HA spheroid invasion in the absence of MMP degradability and RGD for (b) GSC20 and (c) GSC28. Data represent n = 44 [control, RGD (+), and degradable XL (+)], n = 50 [TGF-β, RGD (+), and degradable XL (+)], n = 33 [TGF-β, RGD (+), and degradable XL (−)], n = 32 [TGF-β, RGD (−), and degradable XL (+)] spheroids for GSC20, and n = 31 [control, RGD (+) and degradable XL (+)], n = 28 [TGF-β, RGD (+), and degradable XL (+)], n = 24 [TGF-β, RGD (+), and degradable XL (−)], n = 30 [TGF-β, RGD (−), and degradable XL (+)] spheroids for GSC28. Values display mean ± SEM. *p < 0.033, **p < 0.002, ***p < 0.0002, and ****p < 0.000 01 by Kruskal–Wallis test with Dunn's multiple comparison test. Scale bar: 100 μm.

removed, we observed slower TGF-β stimulated invasion in both GSC20 and GSC28. In the absence of MMP degradabiity, TGF-β-induced invasion decreased by 0.5fold for GSC20 [Fig. 4(b)] and 3.5fold for GSC28 [Fig. 4(c)] compared to when MMP degradability ws present. Surprisingly, TGF-β-induced invasion of GSC20 and GSC28 was nearly completely suppressed when RGD was removed from the HA backbone [Fig. 4(b) and Fig. 4(c)]. Because integrin signaling can strongly affect TGF-β signaling, we asked whether the lack of invasion in RGD-free matrices was directly due to loss of integrin-adhesive function or some broader RGD-dependent dysfunction in TGF-β signaling or matrix invasion capacity. First, we did not detect a difference in TGFBR2 expression between responsive GSCs cultured in HA-RGD (+) and HA-RGD (−) matrices (Fig. S2), implying that loss of RGD did not compromise the ability to bind TGF-β. We then probed expression of genes from our panel of ECM remodeling and GBM mesenchymal genes in GSCs cultured in HA-RGD (−) with and without TGF-β stimulation. We found that transcript expression within the panel mirrored the HA-RGD (+) conditions, in that genes upregulated by TGF-β treatment in the HA-RGD (+) matrix were also upregulated in the HA-RGD (−) matrix [Figs. S3(b), S3(d), S4(b), and S4(d)]. Additionally, we performed qPCR measurements of the same gene set to directly compare TGF-β-treated GSCs cultured in HA-RGD (+) and HA-RGD (−) matrices, which revealed no significant differences (Fig. S5). The results of our qPCR measurements were similar in both TGF-β-responsive GSCs (GSC20 and GSC28). These findings suggest that RGD presentation supports the conversion of transcriptional changes induced by TGF-β treatment into functional invasion of GSCs in the HA matrix.

DISCUSSION

While TGF-β-mediated signaling has been demonstrated to support resistance, stem-like qualities, and tumor-initiating capacity of GSCs, the field's understanding of how TGF-β promotes 3D invasion of GSC-derived tumors remains somewhat limited. This knowledge gap is partially due to a lack of modular 3D culture platforms that enable systematic dissection of cell- and matrix-based regulation of TGF-β during invasion. We show that engineered HA-based matrices can address this unmet need. Using HA-based materials, we successfully classify GSCs into TGF-β-responsive and non-responsive categories and show that TGF-β induces GSC spheroid invasion through SMAD2 phosphorylation. We also show that invasion requires the presentation of integrin ligands (RGD peptides) but surprisingly not MMP-degradable crosslinks.

One important advantage of HA as a platform for studying TGF-β-mediated invasion is that invasion is limited in the absence of TGF-β stimulation, providing a clean "baseline" to assess stimulated invasion in GSCs. This contrasts with collagen I and Matrigel, which support robust invasion even in the absence of exogenous cytokine treatment (Fig. 2). The strong matrix dependence of invasion may be due to the very different architectures of the three matrix systems. Collagen I and Matrigel matrices have been reported to have pore sizes on the order of micrometers, whereas we have reported the pore size of our HA system to be on the nanometer scale.[29,52] Additionally, collagen I hydrogels contain fibers that can be used as contact-guidance cues for rapid invasion. Moreover, Matrigel frequently contains—and collagen I contains binding sites for—pro-migratory cytokines, which could potentially blunt effects of exogenous TGF-β.[29,33,52]

An important advantage of our biomaterial platform is the ability to systematically tune matrix factors to test their influence on invasion, which enabled us to show that the conjugation of RGD peptides to the HA backbone was needed for TGF-β-stimulated invasion (Fig. 4). While the strong integrin dependence of invasion was not perhaps in itself surprising, it was notable that the presence or absence of RGD did strongly influence the expression of nominally pro-invasive genes [Figs. S3 and S4]. This raises the possibility that invasion-competent GSCs are transcriptionally "primed" to invade but cannot execute an invasion program without the appropriate ECM context. This priming hypothesis is supported by two observations in RGD-free matrices: first, integrin expression increases upon stimulation in TGF-β-responsive GSCs; and second, that tumor spheres exhibit jagged edges suggesting increased membrane ruffling (Fig. 4). The strong RGD dependence of invasion raises the question of the role played by HA–CD44 interactions in this system. CD44 expression did not change following TGF-β stimulation [Figs. S3(c) and S4(c)]; however, the interpretation of this finding is complicated by the fact that GSC20 and GSC28 have been reported to have high basal expression of CD44, leaving little dynamic range for a stimulated increase.[8,38] We have also previously reported that CD44-HA is an early and short lived (0.5 h) matrix adhesion system, whereas integrin-based adhesions take longer to mature.[7] Therefore, it is plausible that CD44-HA adhesion alone in RGD-free matrices can initiate but not sustainably support adhesion and adhesion-dependent processes necessary for TGF-β-stimulated invasion over the timescale of invasion (10–14 days).

Finally, our findings add to a growing body of work illustrating the heterogeneity of GSCs with respect to TGF-β sensitivity in other contexts.[18,53,54] GSCs tumors that are responsive to TGF-β *in vivo*, as identified by TGFBR2 expression and phospho-SMAD2, exhibit increased infiltration of immune cells.[53,54] Implications of differential TGF-β sensitivity for invasion have been difficult to dissect *in vivo* due to the complexity of the microenvironment.[18] Our study offers a road-map to tease apart this heterogeneity and further suggests that TGF-β-sensitivity may be cross-correlated with the traditional hierarchy of GBM subtypes (proneural, classical, and mesenchymal). Our study also suggests that changes in SMAD2 phosphorylation status strongly predict TGF-β sensitivity, with SMAD2 phosphorylation not increasing with TGF-β stimulation in non-responsive GSCs. This heterogeneity is consistent both with past studies on the role of TGF-β in inducing mesenchymal transitions and the emerging finding that cells between and within GBM tumors may show characteristics of multiple distinct subtypes, potentially supported by state-switching of GSCs.[18,38,55] It would be valuable to explore these sources of heterogeneity more fully in the future and ask how TGF-β sensitivity maps to other GBM classification categories such as IDH mutation and methylation status. We expect that our HA hydrogel platform and other synthetic invasion platforms can play an important role in reaching these goals.

METHODS
Cell culture

GSC20, GSC28, GSC262, and GSC295 cells were obtained from MD Anderson Cancer Center and propagated as neurospheres in DMEM/F12 basal medium (Corning, Catalog No. 10–090-CV) supplemented with 2% (vol/vol) B-27 supplement (Gibco, 17504-044), 20 ng/ml EGF (R&D Systems, 236-EG-01M), and 20 ng/ml FGF (R&D

Systems, 233-FB-025/CF). For 3D HA gel experiments, the medium was supplemented with 0.1% penicillin/streptomycin (Thermo Fisher Scientific, Catalog No. 15140-122). Cells were screened for mycoplasma and validated by short tandem repeat (STR) analysis every six months.

HA synthesis and RGD conjugation

HA hydrogels were synthesized as previously described.[29] Briefly, methacrylic anhydride (Sigma-Aldrich, 94%, Catalog No. 276685) was used to functionalize sodium hyaluronate (Lifecore Biomedical, Research Grade, 66–99 kDa, HA60K) with methacrylate groups. The extent of methacrylation per disaccharide was quantified by ^{1}H NMR as detailed previously and found to be ∼85% for materials used in this study. For studies involving RGD peptides, methacrylated HA was conjugated via Michael addition with the cysteine-containing RGD peptide Ac-GCGYGRGDSPG-NH2 (Anaspec, Catalog No. AS-62349) at a concentration of 0.5 mmol/l. Peptide crosslinker details are described in the Spheroid Encapsulation sections below.

Generation of spheroids

Glioma stem cell (GSC) spheroids were generated using AggreWell microwell plates (STEMCELL Technologies, Catalog No. 34415). Briefly, the wells of the microwells were treated with a non-adherent rinsing solution (STEMCELL Technologies, Catalog No. 07010). GSCs were then seeded as single cells at ∼200k per well for 2–3 days to allow the cells to aggregate and form uniform tumor spheroids. The spheroids were then encapsulated in hydrogels to perform the 3D spheroid invasion assay. For Matrigel and collagen experiments, cells were seeded ∼300k per well and cultured for 2–3 days.

Spheroid encapsulation in HA

Spheroids were harvested from AggreWell plates, resuspended in non-phenol red DMEM (Thermo Fisher Scientific, Catalog No. 31053028), and mixed with HA hydrogel precursor solution consisting of HA-RGD (+) or HA-RGD (−) polymer, 10 wt. % stock of protease-degradable (KKCGGPQGIWGQGCKK, Genscript) or 10 wt. % stock of non-degradable (KKCGGDQGIAGFGCKK, Genscript) crosslinker containing a bifunctional cysteine peptide. Methacrylated HA was dissolved to a concentration of 1.5 (wt. %/vol. %), and the ratio of thiol: HA monomer was varied to achieve a shear modulus of ∼450 Pa unless mentioned otherwise. Approximately 0.3 thiol:HA monomer ratio was enough to reach the desired shear modulus for both protease-degradable and non-degradable crosslinker. The mixture was then plated as 10 μl droplets in a non-adherent well plate and incubated for 1 h at 37 °C, 5% CO$_2$ before introducing cell culture medium. TGF-β1 ligand (10 ng/ml, R&D Systems, Catalog No. 7754-BH) and Galunisertib 10 μM, Selleckchem, catalog no. S2230) were added to the cell culture medium as needed for each experiment. The medium was changed every 2–4 days.

Spheroid encapsulation in Matrigel

Spheroids were harvested from an AggreWell plate and resuspended in Matrigel (Fisher Scientific, Catalog No. CB40230) at ∼9 mg/ml. The mixture was then plated as droplets in a non-adherent cell culture plate and incubated for 50 min at 37 °C, 5% CO$_2$ before

introducing cell culture medium. TGF-β1 (10 ng/ml, R&D Systems, Catalog No. 7754-BH) was added to the cell culture medium as needed for each experiment.

Spheroid encapsulation in collagen

Spheroids were harvested from an AggreWell plate resuspended in non-phenol red DMEM (Thermo Fisher Scientific) and mixed with bovine collagen type I (Advanced Biomatrix, Catalog No. 5010-50ML), 1N NaOH (Fisher Scientific, LC245004), and 1 N HEPES (Life Technologies, Catalog No. 15630-080) to yield a 2 mg/ml final collagen concentration. The mixture was then plated as droplets in a non-adherent cell culture plate and incubated for 50 min at 37 °C with 5% CO$_2$ before introducing the cell culture medium. TGF-β1 (10 ng/ml, R&D Systems, Catalog No. 7754-BH) was added to the cell culture media as needed for each experiment.

Imaging and spheroid index invasion quantification

Spheroids were tracked for up to 14 days in HA, 24–48 h in Matrigel, and 24 h in collagen using an Eclipse TE2000 Nikon microscope with a Plan Fluor Ph1 × 10 objective. Images were acquired using NIS-Elements Software. Invasion was quantified using ImageJ by outlining the invasion front of the tumor spheroids to acquire a circularity value using the ImageJ function "shape descriptors." The inverse of the circularity was calculated and reported as the spheroid invasion index. A condition where TGF-β was not added was used to normalize the plotted data.

Quantitative real time polymerase chain reaction

Quantitative polymerase chain reaction (qPCR) experiments were set up using paired sample experimental setup and complementary analysis.[56] Cells were dissociated using accutase and encapsulated in the hydrogel at a concentration of 10k cells/10μl of hydrogel for 7 days of culture at 37 °C, 5% CO$_2$. At the end of the culture period, cells encapsulated in the hydrogel were collected from the hydrogel by adding 10k U/ml hyaluronidase (Sigma-Aldrich, Catalog No. H3884) to dissociate the HA hydrogel. Total mRNA was then isolated using TRIzol Reagent (Invitrogen, Catalog No. 15596018) according to manufacturer's recommended protocol. cDNA was synthesized from the isolated mRNA using the IscriptTM cDNA Synthesis Kit (Bio-Rad, Catalog No. 1708891). qPCR was performed using PowerUp Sybr Green Master Mix (Fisher Scientific, Catalog No. A25777) for 40 cycles in a CFX real-time PCR detection system (Bio-Rad). To quantify a relative fold change in the level of genes, qPCR data were analyzed by calculating ΔΔCt with respect to RSP9 as the housekeeping gene. The primer sequences used in this study are listed in supplementary material Table 1.

TCGA and Rembrandt transcriptomic analysis

Human glioma transcriptomic data were obtained from the Rembrandt and The Cancer Genome Atlas (TCGA) patient databases via the GlioVis data portal (http://gliovis.bioinfo.cnio.es/). Using the Rembrandt database, the mRNA expression of TGFBR1, TGFBR2, TGFB1, and TGFB2 from non-tumor, oligodendroglioma, astrocytoma, and glioblastoma tissue was analyzed. mRNA expression levels

in each type of glioma tissue was normalized to non-tumor tissue, and the data were presented as log2(fold change). TCGA was used to extract mRNA expression of TGFBR1, TGFBR2, TGFB1, and TGFB2 from mesenchymal and proneural GBM subtypes. mRNA expression of TGF-β target genes for mesenchymal and proneural subtypes were also extracted from TCGA. mRNA expression of proneural tissues were used to normalize data when comparing mRNA expression of mesenchymal and proneural tumors, and the data were presented as log2(fold change).

Western blot analysis

Cells were cultured for 48 h with or without TGF-β in the 24-well Stem Cell Technology microwell culture plate (Catalog #34811). Six were used, where three wells were treated with TGF-β and three wells were left untreated. After 48 h, cells in each well were harvested and lysed in RIPA buffer (Sigma-Aldrich, Catalog No. R0278) supplemented with Halt protease and phosphatase inhibitor cocktail (Thermo Fisher Scientific, Catalog No. 78442) for protein. Equal masses of protein ($\sim$20 μg) were loaded into each well of a 4%–12% gradient bis-tris gel (Thermo Fisher Scientific), and then blotted onto a nitrocellulose membrane (Licor, Catalog No. 926-31092). Membranes were probed with rabbit anti-SMAD2 antibody (Cell Signaling Technology, Catalog No. 5339) or rabbit anti-pSMAD2 (Cell Signaling Technology, catalog no. 18338T), and mouse anti-β-actin (Sigma-Aldrich, Catalog No. A2228). Blots were then probed with Alexa Fluor 488 goat anti-mouse (Thermo Fisher Scientific, Catalog No. A-11001) or Alexa Fluor 647 goat anti-rabbit (Thermo Fisher Scientific, Catalog No. A-21245a) secondary antibodies. Primary antibodies were diluted at 1:1000, except mouse anti-β-actin (1:15 000). Secondary antibodies were diluted at 1:10 000. Membranes were imaged using iBright imaging system (Invitrogen).

Statistical analysis

Graphical representation and statistical analyses of the data from this study were generated using GraphPad Prism 9. Details of replicates and statistical tests are described in the appropriate figure legends.

SUPPLEMENTARY MATERIAL

See the supplementary material for all supplemental figures referenced in the manuscript and sequences of the qPCR primer used.

ACKNOWLEDGMENTS

AUTHOR DECLARATIONS

Conflict of Interest

The authors have no conflicts to disclose.

Ethics Approval

Ethics approval is not required.

Author Contributions

Kwasi Yeboa Amofa: Conceptualization (equal); Data curation (equal); Formal analysis (equal); Writing – original draft (equal); Writing – review & editing (equal). **Katherine Michelle Patterson:** Data curation (equal); Formal analysis (equal). **Jessica Ortiz:** Data curation (supporting); Formal analysis (supporting). **Sanjay Kumar:** Conceptualization (equal); Funding acquisition (equal); Supervision (equal); Writing – review & editing (equal).

DATA AVAILABILITY

The data that support the findings of this study are available from the corresponding author upon reasonable request.

REFERENCES

[1]G. F. Beeghly, K. Y. Amofa, C. Fischbach, and S. Kumar, "Regulation of tumor invasion by the physical microenvironment: Lessons from breast brain cancer," Annu. Rev. Biomed. Eng. **24**, 29–59 (2022).

[2]K. J. Wolf, J. Chen, J. D. Coombes, M. K. Aghi, and S. Kumar, "Dissecting and rebuilding the glioblastoma microenvironment with engineered materials," Nat. Rev. Mater. **4**, 651–668 (2019).

[3]E. C. F. Yeo, M. P. Brown, T. Gargett, and L. M. Ebert, "The role of cytokines and chemokines in shaping the immune microenvironment of glioblastoma: implications for immunotherapy," Cells **10**, 607 (2021).

[4]S. J. Coniglio and J. E. Segall, "Review: Molecular mechanism of microglia stimulated glioblastoma invasion," Matrix Biol. **32**, 372–380 (2013).

[5]E. A. Akins, M. K. Aghi, and S. Kumar, "Incorporating tumor-associated macrophages into engineered models of glioma," iScience **23**, 101770 (2020).

[6]J. Winkler, A. Abisoye-Ogunniyan, K. J. Metcalf, and Z. Werb, "Concepts of extracellular matrix remodelling in tumour progression and metastasis," Nat. Commun. **11**, 5120 (2020).

[7]Y. Kim and S. Kumar, "CD44-mediated adhesion to hyaluronic acid contributes to mechanosensing and invasive motility," Mol. Cancer Res. **12**, 1416–1429 (2014).

[8]K. J. Wolf et al., "A mode of cell adhesion and migration facilitated by CD44-dependent microtentacles," Proc. Natl. Acad. Sci. U. S. A. **117**, 11432–11443 (2020).

[9]P. G. Gritsenko and P. Friedl, "Adaptive adhesion systems mediate glioma cell invasion in complex environments," J. Cell Sci. **131**, jcs216382 (2018).

[10]L. Cheng et al., "Elevated invasive potential of glioblastoma stem cells," Biochem. Biophys. Res. Commun. **406**, 643–648 (2011).

[11]J. D. Lathia, S. C. Mack, E. E. Mulkearns-Hubert, C. L. L. Valentim, and J. N. Rich, "Cancer stem cells in glioblastoma," Genes Dev. **29**, 1203–1217 (2015).

[12]P. Ruiz-Ontañon et al., "Cellular plasticity confers migratory and invasive advantages to a population of glioblastoma-initiating cells that infiltrate peritumoral tissue," Stem Cells **31**, 1075–1085 (2013).

[13]G. Frosina, "DNA repair and resistance of gliomas to chemotherapy and radiotherapy," Mol. Cancer Res. **7**, 989–999 (2009).

[14]A. M. Bleau et al., "PTEN/PI3K/Akt pathway regulates the side population phenotype and ABCG2 activity in glioma tumor stem-like cells," Cell Stem Cell **4**, 226–235 (2009).

[15]G. Liu et al., "Analysis of gene expression and chemoresistance of CD133^{+} cancer stem cells in glioblastoma," Mol. Cancer **5**, 67 (2006).

[16]M. E. Hardee et al., "Resistance of glioblastoma-initiating cells to radiation mediated by the tumor microenvironment can be abolished by inhibiting transforming growth factor-β," Cancer Res. **72**, 4119–4129 (2012).

[17]H. Ikushima et al., "Autocrine TGF-β signaling maintains tumorigenicity of glioma-initiating cells through Sry-related HMG-box factors," Cell Stem Cell **5**, 504–514 (2009).

[18]J. V. Joseph et al., "TGF-β is an inducer of ZEB1-dependent mesenchymal transdifferentiation in glioblastoma that is associated with tumor invasion," Cell Death Dis. **5**, e1443 (2014).

[19]T. Yan et al., "TGF-β induces GBM mesenchymal transition through upregulation of CLDN4 and nuclear translocation to activate TNF-α/NF-κB signal pathway," Cell Death Dis. **13**, 339 (2022).

[20]J. V. Joseph et al., "TGF-β promotes microtube formation in glioblastoma through thrombospondin 1," Neuro-Oncology **24**, 541–553 (2022).

[21]J. Lee et al., "Tumor stem cells derived from glioblastomas cultured in bFGF and EGF more closely mirror the phenotype and genotype of primary tumors than do serum-cultured cell lines," Cancer Cell **9**, 391–403 (2006).

[22]S. S. Nazari, "Generation of 3D tumor spheroids with encapsulating basement membranes for invasion studies," Curr. Protoc. Cell Biol. **87**, e105 (2020).

[23]S. R. Caliari and J. A. Burdick, "A practical guide to hydrogels for cell culture," Nat. Methods **13**, 405–414 (2016).

[24]A. K. Gaharwar, I. Singh, and A. Khademhosseini, "Engineered biomaterials for in situ tissue regeneration," Nat. Rev. Mater. **5**, 686–705 (2020).

[25]E. M. Carvalho and S. Kumar, "Lose the stress: Viscoelastic materials for cell engineering," Acta Biomater. **163**, 146–157 (2023).

[26]B. Delpech et al., "Hyaluronan and hyaluronectin in the extracellular matrix of human brain tumour stroma," Eur. J. Cancer **29**, 1012–1017 (1993).

[27]K. J. Wolf and S. Kumar, "Hyaluronic acid: Incorporating the bio into the material," ACS Biomater. Sci. Eng. **5**, 3753 (2019).

[28]L. J. Smith et al., "Engineered in vitro tumor model recapitulates molecular signatures of invasion in glioblastoma," ACS Mater. Au **3**, 514–527 (2023).

[29]B. Ananthanarayanan, Y. Kim, and S. Kumar, "Elucidating the mechanobiology of malignant brain tumors using a brain matrix-mimetic hyaluronic acid hydrogel platform," Biomaterials **32**, 7913–7923 (2011).

[30]K. J. Wolf, S. Lee, and S. Kumar, "A 3D topographical model of parenchymal infiltration and perivascular invasion in glioblastoma," APL Bioeng. **2**, 031903 (2018).

[31]W. Xiao et al., "Bioengineered scaffolds for 3D culture demonstrate extracellular matrix-mediated mechanisms of chemotherapy resistance in glioblastoma," Matrix Biol. **85–86**, 128–146 (2020).

[32]J. H. Garcia et al., "Multiomic screening of invasive GBM cells reveals targetable transsulfuration pathway alterations," J. Clin. Invest. **134**, e170397 (2024).

[33]A. Sohrabi et al., "Microenvironmental stiffness induces metabolic reprogramming in glioblastoma," Cell Rep. **42**, 113175 (2023).

[34]T. Ito, J. D. Williams, D. J. Fraser, and A. O. Phillips, "Hyaluronan regulates transforming growth factor-β1 receptor compartmentalization," J. Biol. Chem. **279**, 25326–25332 (2004).

[35]T. Ito, J. D. Williams, D. Fraser, and A. O. Phillips, "Hyaluronan attenuates transforming growth factor-β1-mediated signaling in renal proximal tubular epithelial cells," Am. J. Pathol. **164**, 1979–1988 (2004).

[36]L. Y. W. Bourguignon, P. A. Singleton, H. Zhu, and B. Zhou, "Hyaluronan promotes signaling interaction between CD44 and the transforming growth factor β receptor I in metastatic breast tumor cells," J. Biol. Chem. **277**, 39703–39712 (2002).

[37]F. Wang, H. M. Chang, Y. Yi, H. Li, and P. C. K. Leung, "TGF-β1 promotes hyaluronan synthesis by upregulating hyaluronan synthase 2 expression in human granulosa-lutein cells," Cell Signal **63**, 109392 (2019).

[38]K. P. L. Bhat et al., "Mesenchymal differentiation mediated by NF-κB promotes radiation resistance in glioblastoma," Cancer Cell **24**, 331–346 (2013).

[39]T. Daubon et al., "Deciphering the complex role of thrombospondin-1 in glioblastoma development," Nat. Commun. **10**, 1146 (2019).

[40]M. Khoonkari, D. Liang, M. Kamperman, F. A. E. Kruyt, and P. van Rijn, "Physics of brain cancer: Multiscale alterations of glioblastoma cells under extracellular matrix stiffening," Pharmaceutics **14**, 1031 (2022).

[41]J. M. Barnes, L. Przybyla, and V. M. Weaver, "Tissue mechanics regulate brain development, homeostasis and disease," J. Cell Sci. **130**, 71 (2017).

[42]S. Budday, T. C. Ovaert, G. A. Holzapfel, P. Steinmann, and E. Kuhl, "Fifty Shades of brain: A review on the mechanical testing and modeling of brain tissue," Arch. Comput. Methods Eng. **27**, 1187–1230 (2020).

[43]A. C. Bellail, S. B. Hunter, D. J. Brat, C. Tan, and E. G. Van Meir, "Microregional extracellular matrix heterogeneity in brain modulates glioma cell invasion," Int. J. Biochem. Cell Biol. **36**, 1046–1069 (2004).

[44]A. Passaniti, H. K. Kleinman, and G. R. Martin, "Matrigel: History/background, uses, and future applications," J. Cell Commun. Signal **16**, 621–626 (2022).

[45]D. Capper et al., "Biomarker and histopathology evaluation of patients with recurrent glioblastoma treated with galunisertib, lomustine, or the combination of galunisertib and lomustine," Int. J. Mol. Sci. **18**, 995 (2017).

[46]J. E. Murphy-Ullrich and M. J. Suto, "Thrombospondin-1 regulation of latent TGF-β activation: A therapeutic target for fibrotic disease," Matrix Biol. **68–69**, 28 (2018).

[47]N. R. Park et al., "Synergistic effects of CD44 and TGF-β1 through AKT/GSK-3β/β-catenin signaling during epithelial-mesenchymal transition in liver cancer cells," Biochem. Biophys. Res. Commun. **477**, 568–574 (2016).

[48]S. A. Park et al., "TIMP-1 mediates TGF-β-dependent crosstalk between hepatic stellate and cancer cells via FAK signaling," Sci. Rep. **5**, 16492 (2015).

[49]Q. C. Qiu et al., "CHI3L1 promotes tumor progression by activating TGF-β signaling pathway in hepatocellular carcinoma," Sci. Rep. **8**, 15029 (2018).

[50]T. Wang, H. Lu, D. Li, and W. Huang, "TGF-β1-mediated activation of SERPINE1 is involved in hemin-induced apoptotic and inflammatory injury in HT22 cells," Neuropsychiatr. Dis. Treat. **17**, 423 (2021).

[51]J. Behnan, G. Finocchiaro, and G. Hanna, "The landscape of the mesenchymal signature in brain tumours," Brain **142**, 847–866 (2019).

[52]M. H. Zaman et al., "Migration of tumor cells in 3D matrices is governed by matrix stiffness along with cell-matrix adhesion and proteolysis," Proc. Natl. Acad. Sci. U. S. A. **103**, 10889–10894 (2006).

[53]C. P. Beier et al., "The cancer stem cell subtype determines immune infiltration of Glioblastoma," Stem Cells Dev. **21**, 2753–2761 (2012).

[54]A. Wesolowska et al., "Microglia-derived TGF-β as an important regulator of glioblastoma invasion—An inhibition of TGF-β-dependent effects by shRNA against human TGF-β type II receptor," Oncogene **27**, 918–930 (2008).

[55]C. Neftel et al., "An integrative model of cellular states, plasticity, and genetics for glioblastoma," Cell **178**, 835–849 (2019).

[56]M. T. Ganger, G. D. Dietz, and S. J. Ewing, "A common base method for analysis of qPCR data and the application of simple blocking in qPCR experiments," BMC Bioinf. **18**, 534 (2017).